blood

American Society of Hematology
2021 L Street NW, Suite 900,
Washington, DC 20036
Phone: 202-776-0544 | Fax 202-776-0545
editorial@hematology.org

Chromosome 5q deletion drives evolution of aneuploidy in myeloid neoplasms with complex karyotype

Tracking no: BLD-2025-031996R2

J. Philip Creamer (Columbia University Medical Center, United States) Suhita Ray (Columbia University Medical Center, United States) Sintra Stewart (University of Washington, United States) Suleyman Gulsuner (University of Washington, United States) Antoine Saliba (Mayo Clinic, United States) Jieya Wu (City of Hope National Medical Center, United States) Frank Huang (German Cancer Research Center, Germany) Aino-Maija Leppä (Francis Crick Institute, United Kingdom) Bofei Wang (The University of Texas MD Anderson Cancer Center, United States) Hussein Abbas (M D Anderson Cancer Center, United States) Janis Abkowitz (University of Washington, United States) Jacob Appelbaum (Fred Hutch Cancer Center, United States) Scott Kaufmann (Mayo Clinic, United States) Pamela Becker (City Of Hope National Medical Center, United States) Andreas Trumpp (German Cancer Research Center, Germany) Vaidehi Jobanputra (Columbia University Medical Center,) Min Fang (Fred Hutchinson Cancer Research Center, United States) Elizabeth Swisher (University of Washington, United States) Sergei Doulatov (Columbia University Medical Center, United States)

Abstract:
Clonal acquisition of multiple chromosomal abnormalities in hematopoietic stem and progenitor cells (HSPCs) is a hallmark of high-risk acute myeloid leukemias with complex karyotype (AML-CK). AML-CK is associated with TP53 mutations and chromosome 5q deletions (del5q); however, the drivers and clonal trajectories of aneuploid evolution in HSPCs remain unknown. We have developed a patient-derived induced pluripotent stem cell (iPSC) model in which preleukemic HSPCs clonally evolve to distinct, highly aneuploid states following transient mitotic inhibition. By tracking chromosome evolution at single cell resolution, we show that TP53-mutant HSPCs with del5q, but not TP53 mutation alone, evolved complex chromosomal changes. Clonal evolution was marked by stepwise acquisition of numerical and structural chromosome changes seen in AML-CK patients, with individual abnormalities conferring fitness advantage. iPSC-derived aneuploid HSPCs and primary AML-CK patient samples exhibited a conserved gene expression signature marked by upregulation of PTEN, cohesins, and anti-apoptotic factor BCL2, indicative of a shared aneuploid cell state in HSPCs. Clinical BCL2 inhibitor venetoclax eradicated BCL2-dependent aneuploid clones, with resistant clones undergoing a lineage switch to upregulate alternative BCL2 factors. In summary, we demonstrate that mutant TP53 and del5q drive chromosome evolution marked by stepwise acquisition of individual abnormalities. Moreover, aneuploid HSPCs exhibit a shared gene expression state which confers unique targetable therapeutic vulnerabilities in AML-CK.

Conflict of interest: COI declared - see note

COI notes: H.A.A. received honorarium and in-kind support from Illumina. The other authors declare no potential conflicts of interest.

Preprint server: No;

Author contributions and disclosures: J.P.C., and S.D. conceived the project and designed the experiments; J.P.C., performed the experiments with help from S.R., S.S., V.J., and J.W.; J.P.C., S.R., S.G., F.Y.H., AM.L., V.J., P.S.B, A.T., M.F., E.M.S., and S.D., analyzed and interpreted the data; J.L.A., J.S.A., S.H.K., P.S.B, A.T., V.J., M.F., and E.M.S., provided input on experimental design and interpretation. B.W., and H.A.A. provided patient sample data. A.N.S., S.H.K., J.S.A., J.L.A., and E.M.S., provided patient samples and clinical interpretation; J.P.C., and S.D. prepared the manuscript.

Non-author contributions and disclosures: No;

Agreement to Share Publication-Related Data and Data Sharing Statement: Raw and processed single cell RNA sequencing data and CNI analysis have been deposited to Gene Expression Omnibus (GEO) under accession #GSE282370.

Clinical trial registration information (if any):

Chromosome 5q deletion drives evolution of aneuploidy in myeloid neoplasms with complex karyotype

J. Philip Creamer [1,2], Suhita Ray [1,2], Sintra Stewart [2], Suleyman Gulsuner [3], Antoine N. Saliba [4], Jieya Wu [5,6], Frank Y. Huang [7,8], Aino-Maija Leppä [7,8,9], Bofei Wang [10], Hussein A. Abbas [10,11], Janis L. Abkowitz [2,12,13], Jacob S. Appelbaum [2,14], Scott H. Kaufmann [4,15], Pamela S. Becker [5,6], Andreas Trumpp [7,8,16], Vaidehi Jobanputra [17,18], Min Fang [14,19], Elizabeth M. Swisher [20], Sergei Doulatov [1,2,13,21]

[1]Department of Physiology and Cellular Biophysics, Columbia University Irving Medical Center, New York, NY
[2]Division of Hematology and Oncology, Department of Medicine, University of Washington, Seattle, WA
[3]Division of Medical Genetics, Department of Medicine, University of Washington, Seattle, WA
[4]Division of Hematology, Department of Medicine, Mayo Clinic, Rochester, MN
[5]Department of Hematology and Hematopoietic Cell Transplantation, City of Hope National Medical Center, Duarte, CA
[6]Department of Hematologic Malignancies Translational Science, City of Hope Beckman Research Institute, Duarte, CA
[7]Division of Stem Cells and Cancer, German Cancer Research Center (DKFZ), Heidelberg, Germany
[8]Heidelberg Institute of Stem Cell Technology and Experimental Medicine (HI-STEM gGmbH), Heidelberg, Germany
[9]Cancer Evolution and Genome Instability Laboratory, Francis Crick Institute, London, UK
[10]Department of Leukemia, The University of Texas MD Anderson Cancer Center, Houston, TX
[11]Department of Genomic Medicine, Division of Cancer Medicine, The University of Texas MD Anderson Cancer Center, Houston, TX, USA
[12]Institute for Stem Cell and Regenerative Medicine, University of Washington, Seattle, WA
[13]Department of Genome Sciences, University of Washington, Seattle, WA
[14]Clinical Research Division and Translational Science and Therapeutics Division, Fred Hutch Cancer Center, Seattle, WA
[15]Department of Molecular Pharmacology and Experimental Therapeutics, Mayo Clinic, Rochester, MN
[16]German Cancer Consortium (DKTK), Heidelberg, Germany
[17]Department of Pathology, Columbia University Irving Medical Center, New York, NY
[18]New York Genome Center, New York, NY
[19]Department of Laboratory Medicine and Pathology, University of Washington, Seattle, WA
[20]Division of Gynecologic Oncology, University of Washington School of Medicine, WA
[21]Herbert Irving Comprehensive Cancer Center, Columbia University Medical Center, New York, NY

Corresponding author:
Sergei Doulatov
Columbia University
sd3923@cumc.columbia.edu

Running title: 5q deletion drives evolution of aneuploidy

Category: Myeloid neoplasia
Word Count: 4396
Figure Count: 6 Figures, 1 Table
Reference Count: 58

Data sharing statement: Raw and processed single cell RNA sequencing data and CNI analysis have been deposited to Gene Expression Omnibus (GEO) under accession #GSE282370.

Key Points

- Chromosome 5q deletion drives progressive chromosome evolution in *TP53*-mutant preleukemic HSPCs.
- Aneuploid HSPCs exhibit a shared gene expression signature which confers unique therapeutic vulnerabilities in AML-CK.

Abstract

Clonal acquisition of multiple chromosomal abnormalities in hematopoietic stem and progenitor cells (HSPCs) is a hallmark of high-risk acute myeloid leukemias with complex karyotype (AML-CK). AML-CK is associated with *TP53* mutations and chromosome 5q deletions (del5q); however, the drivers and clonal trajectories of aneuploid evolution in HSPCs remain unknown. We have developed a patient-derived induced pluripotent stem cell (iPSC) model in which preleukemic HSPCs clonally evolve to distinct, highly aneuploid states following transient mitotic inhibition. By tracking chromosome evolution at single cell resolution, we show that *TP53*-mutant HSPCs with del5q, but not *TP53* mutation alone, evolved complex chromosomal changes. Clonal evolution was marked by stepwise acquisition of numerical and structural chromosome changes seen in AML-CK patients, with individual abnormalities conferring fitness advantage. iPSC-derived aneuploid HSPCs and primary AML-CK patient samples exhibited a conserved gene expression signature marked by upregulation of *PTEN,* cohesins, and anti-apoptotic factor *BCL2*, indicative of a shared aneuploid cell state in HSPCs. Clinical BCL2 inhibitor venetoclax eradicated BCL2-dependent aneuploid clones, with resistant clones undergoing a lineage switch to upregulate alternative BCL2 factors. In summary, we demonstrate that mutant *TP53* and del5q drive chromosome evolution marked by stepwise acquisition of individual abnormalities. Moreover, aneuploid HSPCs exhibit a shared gene expression state which confers unique targetable therapeutic vulnerabilities in AML-CK.

Introduction

Aneuploidy involves changes in chromosome number or structure[1-3] and is pervasive in cancers[4]. Aneuploidy is a hallmark of high-risk acute myeloid leukemias (AML) with complex karyotype (AML-CK), defined as three or more chromosomal abnormalities[5]. AML-CK is almost universally associated with mutations in *TP53*, very poor outcomes, and lower response to current antileukemic therapies[6-8]. Most AML-CK patients present with widespread aneuploidy at diagnosis, making it challenging to reconstruct clonal trajectories of early disease. It remains unknown how hematopoietic stem and progenitor cells (HSPCs) with aneuploidy first arise and evolve, ultimately giving rise to these aggressive leukemias.

While relatively infrequent in *de novo* AML, complex karyotype with *TP53* mutations is enriched in therapy-related myeloid neoplasms (t-MN), implicating cytotoxic therapy in inducing chromosome instability or creating selective pressure for the mutant clones[9]. *TP53* mutant clones are detectable at low frequency years prior to t-MN diagnosis, and in many cases are antecedent to chemotherapy[10,11]. *TP53* mutations are found in age-related clonal hematopoiesis, which is associated with an increased risk of myeloid malignancy[12,13]. These observations broadly suggest that *TP53* mutations are early events in AML-CK pathogenesis, and that clonal progression to AML-CK requires the occurrence of additional genetic events often in the context of cytotoxic therapy. Despite the advent of improved single cell copy number detection methods, detection of early clones in this disease remains rare[14]. Consequently, little is known about the genetic drivers and trajectories of AML-CK evolution from preleukemic HSPCs.

Specific chromosomal abnormalities are recurrently observed in certain cancers, suggesting that they impact genes that contribute to cancer fitness and progression[15,16]. Most patients with AML-CK harbor recurrent deletions on chromosomes 5q (del5q), 7q, and/or 17p (encoding *TP53*), with del(5q) being the most common change found in over 80% of AML-CK cases, suggesting that this region encodes critical genes for disease progression[7,17-19]. Classical studies have established the contribution of individual 5q genes to leukemogenesis[19-23]. However, it remains unknown if 5q deletion acts as a driver of AML-CK progression, owing to lack of experimental model systems in which normal HSPCs evolve to complex karyotypes. Understanding the role of del5q as a driver in AML-CK could nominate mechanisms and molecular dependencies due to haploinsufficiency of 5q-encoded genes. Aneuploid states more broadly may confer specific molecular dependencies due to cellular stresses on proteostasis, replication, and mitosis[24], which could be therapeutically harnessed for incurable *TP53*-mutated leukemias[25].

Here we report an induced pluripotent stem cell (iPSC) model in which patient-derived *TP53*-mutant preleukemic HSPCs evolve to distinct highly aneuploid states following mitotic mis-segregation. We show that HSPCs with *TP53* mutation and del5q undergo progressive aneuploid evolution resembling AML-CK

patients. By tracking the trajectories of chromosome evolution at the single cell level, we show that aneuploid evolution is characterized by stepwise acquisition of abnormalities which converged on shared gene expression signature with AML-CK patients, revealing unique molecular dependencies associated with acquisition of aneuploidy in HSCs which can be therapeutically targeted in *TP53*-mutated leukemias.

Materials and Methods

MDS/AML iPSC-derived HSPC culture. *TP53*^{mut} and *TP53*^{mut} del5q iPSC lines were previously derived from bone marrow cells of a female MDS/AML-CK patient[20,26]. Primary AML samples were obtained from the Fred Hutchinson Cancer Center Co-Operative Center for Excellence in Hematology core or the Mayo Clinic Biorepository for Acute Leukemia Research after Institutional Review Board approval. Written informed consent was obtained from all participants. iPSC lines were differentiated into HSPCs, and established as expandable iPSC-HSPCs by the introduction of five transcription factors[20,26]. iPSC-HSPCs were cultured in StemSpan SFEM II (StemCell Technologies) plus 50 ng/mL SCF, 50 ng/ml FLT3, 50 ng/ml TPO, 50 ng/ml IL-6, 10 ng/ml IL-3 (Peprotech), and doxycycline (2 µg/ml) (Sigma)[27]. Cells were maintained at 0.5-1x10^6 cells/ml and media changed every 3 to 4 days. For evolution to aneuploidy, iPSC-HSPC cell lines were treated with 1 µM of NMS-P715 MPS1 inhibitor (Sigma) in DMSO for 24 hours, followed by a complete media change. Cultures were maintained at 0.5-1x10^6 cells/ml and cultured for 60-70 days or as specified. Complete details are provided in Supplementary Methods.

Single cell RNA sequencing and CNI analysis. Patient samples were thawed by dropwise addition of IMDM + 1% BSA, washed, and then purified using the CD34+ MACS (Miltenyi) selection column, followed by the Dead Cell Removal Kit (Miltenyi). iPSC-HSPC cell lines were thawed and dead cells removed by the Dead Cell Removal Kit. Single cell sequencing was performed using the 10X Chromium Next GEM Single Cell 3' Reagents kit v.3.1 on a Chromium Controller. Libraries were sequenced using Illumina NGS NextSeq/NovaSeq 150/100 PE cycle kits. After alignment to hg38 using the 10X genomics Cell Ranger count tool, the Seurat R Package[28] v4.1.3 was used to perform integration where multiple runs were analyzed together, with mitochondrial gene regression (SCTransform function), dimensional reduction, UMAP generation, and clustering. Copy number inference was performed using the Numbat package[29]. Complete details are provided in Supplementary Methods.

Data Availability

Raw and processed single cell RNA sequencing data and CNI analysis have been deposited to GEO under accession #GSE282370.

Results

Experimental model of aneuploid evolution in preleukemic HSPCs

We have previously reprogrammed bone marrow cells from a Li-Fraumeni patient who developed AML-CK and isolated two isogenic preleukemic iPSC lines: an ancestral line with a heterozygous *TP53* R209fs mutation (herein *TP53*^{mut}), and a derived line with *TP53* R209fs and an isolated del(5)(q22q31) (herein *TP53*^{mut}del5q)[20,26]. Reprogramming of these clones suggested that *TP53*-mutant preleukemic clones first acquired isolated del(5q), followed by other complex abnormalities (which were not compatible with reprogramming). We differentiated *TP53*^{mut} and *TP53*^{mut}del5q iPSCs to CD34^{+} HSPCs and established conditionally immortalized HSPCs, which can be continuously expanded for ~5 months while maintaining a developmental hierarchy with multipotent CD34^{+} HSPCs and more differentiated myeloid cell types[20,26]. *TP53*^{mut} and *TP53*^{mut}del5q HSPCs expanded with similar cell division characteristics and maintained a stable karyotype over extended culture (**Figure 1A**; **Supplementary Figure 1A-B**).

Errors in chromosome segregation due to defective mitotic checkpoint is a major mechanism of chromosome instability in cancers[3,30]. MPS1 kinase inhibitors (MPSi) robustly induce chromosome mis-segregation giving rise to aneuploid clones[31-33]. We transiently treated *TP53*^{mut} and *TP53*^{mut}del5q HSPCs with the MPSi NMS-P715 for 24 hours and monitored by conventional karyotyping over extended 5 to 10-week culture (**Figure 1A**). Strikingly, we observed robust evolution to distinct highly aneuploid states following MPSi treatment across multiple experiments. Even more surprisingly, *TP53*^{mut}del5q HSPCs almost invariably evolved to aneuploidy (mean ~95.1%), whereas parental *TP53*^{mut} HSPCs infrequently gave rise to aneuploid clones (mean = 5.8%) ($p<0.0001$) (**Figure 1B**). *TP53*^{mut}del5q cultures harbored a greater number of abnormalities per clone ($p=0.0002$) and distinct clones ($p<0.0001$) compared to *TP53*^{mut} HSPCs (**Figure 1C,D**). The clones derived from *TP53*^{mut}del5q HSPCs typically gained ~2 additional abnormalities, with several subclones observable by conventional karyotyping (at least 2 out of 20 cells counted) after ~5 weeks of culture (**Table 1**). The abnormalities observed in the *TP53*^{mut}del5q MPSi culture were reflective of patients with AML-CK, including trisomy 8 (+8), trisomy 10 (+10), and unbalanced translocations or deletions of chromosome 21 (chr. 21) (**Figure 1E**; **Table 1**; **Supplementary Table 1**). These observations contrasted with *TP53*^{mut} HSPCs, which never reached >20% of total culture (**Figure 1B**). Taken together our findings show that iPSC-derived HSPCs undergo robust chromosome evolution upon mitotic checkpoint inhibition and that 5q loss is a cooperating abnormality required for complex karyotype evolution.

Evolution of aneuploidy is a stepwise process shaped by clonal competition

The clonal trajectories by which preleukemic *TP53*-mutant HSPCs evolve to aneuploidy in AML-CK are unknown. To examine these evolutionary dynamics, we followed paired *TP53*^{mut}del5q "evolving" and

TP53^{mut} "non-evolving" HSPCs in long-term culture following segregation error (**Figure 2A**). In a representative experiment, 3 independent *TP53*^{mut}del5q subclones emerged ~1 month after MPSi treatment with additional material on chr. 21 [del(5q),add(21p)], monosomy 21 [del(5q),-21], and trisomy 10 [del(5q),+10] (**Figure 2B**, top; **Supplementary Figure 2A**, left). After another month in culture, the add(21p) emerged as the dominant clone reaching fixation (~100%), with the other clones no longer detectable by conventional karyotyping (**Figure 2B**, top). Interestingly, the add(21p) clone further diversified by acquiring add(11p), not detected at the previous time point (**Figure 2B**; **Supplementary Figure 2A**, middle). The paired *TP53*^{mut} culture exhibited limited karyotype changes, with the presence of a minor +8 clone at ~10% (**Supplementary Figure 2B**). Whole genome sequencing showed that a limited number of single nucleotide variants were acquired during aneuploid evolution that were private to individual lines and did not map to known cancer driver genes (**Supplementary Table 2**). These data suggest that chromosome evolution is driven by clonal competition, with a single clone emerging as the "winner" and further gradually diversifying.

The initial mis-segregation event is expected to produce small numbers of abnormal clones which may be lost by genetic drift. To test this possibility, we set up a parallel culture from a cryopreserved sample immediately after MPSi treatment (**Figure 2A**). By repeating the evolution experiment, we observed a completely different winning clone with deletion 1p [del(5q),del(1p),dup(2),-21] gaining dominance over the add(21p) clone, the latter failing to further diversify (**Figure 2B**; bottom; **Supplementary Figure 2A**, right). One possible explanation is the bottleneck effect, wherein the rare del(1p) clone was randomly split into the cryopreserved sample. To determine if individual abnormalities act as drivers, we estimated the relative fitness of each clone using a Bayesian probabilistic framework designed to fit existing clone frequency measurements over time[34]. Notably, add(21p) clone had a relative fitness advantage (mean 1+s ~1.014) in the original culture in which the del(1p) clone was not detected (**Figure 2C**, top). By contrast, its fitness advantage was lost in the repeat culture (mean 1+s ~0.971) (**Figure 2C**, bottom). These data suggest that certain chromosome abnormalities act as drivers to confer highest relative fitness, with the repertoire of competing clones shaped by genetic drift and clonal selection.

To better examine evolutionary dynamics in early culture, we modeled a long-term evolution experiment[35,36] by splitting an initial culture into four separate sub-cultures (A-D) after the 24-hour MPSi treatment (**Figure 2D**). We observed multiple competing subclones in the four cultures, notably distinct from the ones seen in the previous experiment, followed by emergence of the +8 founder as the "winning" clone in all cultures (**Figure 2E**). Interestingly, the +8 clone further diversified by acquiring unique abnormalities in each culture, including add(11), +19, or +10 (**Figure 2E**). We observed some diversification of the founding clone in *TP53*^{mut} cultures, but with limited selection (**Supplementary Figure 2C**). Mixing of the cultures after ~2 weeks resulted in a similar pattern of clonal expansion of the

+8 founder (**Supplementary Figure 2D**). Estimates of relative fitness (1+s) varied for each sub-culture, but were consistent with +8 acting as the driver event (**Figure 2F**). Taken together, these data suggest that AML-CK evolution is shaped by genetic drift limiting the initial repertoire of aberrant clones, with clonal competition selecting a winning founder clone with the highest relative fitness, with subsequent evolution of progressively fitter clones. These findings help explain the highly variable karyotypes of individual AML-CK patients, which often contain derivatives of a single dominant clone (e.g., stemline).

Single cell analysis identifies gene expression signature of aneuploidy

Conventional cytogenetic analysis is a gold standard in clinical practice but limited to manual examination of a small number of metaphases. To gain deeper insight into the clonal dynamics and concurrent cell state changes, we utilized single cell RNAseq to quantify changes in gene expression in aneuploid clones identified by copy number inference (CNI)[29,37]. We profiled sequential samples in the representative experiment in Figure 2A by single cell transcriptomics, followed by haplotype-aware copy number calling (**Figure 3A**; **Supplementary Figure 3A**). As validation, unbiased calling of del(5q) in a combined *TP53*^{mut} and *TP53*^{mut}del5q dataset revealed >95% confidence in correct calling (**Supplementary Figure 3B**). Consistent with conventional karyotyping, *TP53*^{mut} culture was comprised of several clones at <10% frequency, whereas *TP53*^{mut}del5q culture reached ~60% abnormal cells (**Figure 3B**; **Supplementary Figure 3C**). Unbiased lineage reconstruction further identified distinct normal and del(5q) clonal branches (**Figure 3C**). Analysis of *TP53*^{mut}del5q culture by conventional karyotyping showed the winning add(21p) clone (**Figure 2B**), but surprisingly, no chr. 21 abnormalities were called by CNI. Instead, gain of chr. 10q material (10q+) was identified (**Figure 3C**), suggesting that the additional material on chr. 21p was derived from 10q. To confirm this, whole genome sequencing identified a gain of 10q22qter including the *PTEN* gene, which was localized to chr. 21p by metaphase FISH (**Supplementary Figure 3D,E**). These data show that single cell CNI enables robust identification of aneuploid clones, with improved ability to define the origin of rearranged material.

We next sought to define the gene expression changes associated with acquisition of aneuploidy in HSPCs. To this end, we compared gene expression between the ancestral del(5q) and the derived 10q+/add(21p) clone identified by CNI. Both cell types shared a similar distribution of myeloid, lymphoid, and progenitor cell populations (**Supplementary Figure 3F**; **Supplementary Table 3**). We identified 272 differentially expressed genes, including 116 upregulated genes, of which 37 were encoded within the 10q+ interval (**Supplementary Table 4**)[38]. Upregulated genes included the 10q *PTEN* tumor suppressor, which has an essential role in genome integrity[39,40], anti-apoptotic factor *BCL2*, and *CD34* (**Figure 3D**). Upregulated genes were enriched for gene ontology terms related to mitosis and cohesin loading, TGFβ pathway, p53 pathway, apoptotic signaling, and cell cycle (**Figure 3E**). Key mitotic factors included cohesin subunits *STAG1*, *STAG2*, *WAPL*, and *SMC3*, regulators of sister chromatid segregation *CENPF*,

KIF11, *KIF20B*, *TOP2A*, and genome integrity factors *SHLD2*, *HELLS,* and *PTEN* (**Figure 3D; Supplementary Table 4**), many of which are encoded in the 10q+ interval. These alterations suggest that aneuploid HSPCs upregulate chromosome segregation factors which may facilitate the maintenance of aneuploid cell state.

Aneuploidy signature is shared with AML-CK patients

To determine if these gene expression changes are broadly associated with aneuploidy in hematopoietic cells, we next performed single cell transcriptomics on two primary AML-CK patient samples with *TP53* mutation and del(5q) (**Figure 4A**). CNI analysis of patient RO20518 identified del(5q) [add(5)(q11.2)], +8, chr. 15 abnormalities [t(2;15)], and -16, found in the clinical karyotype (**Figure 4B**; **Supplementary Table 5**). CNI analysis of patient R332 identified -5, -7, +8, +19, +21, and +22 identified in karyotype analysis (**Supplementary Figure 4A; Supplementary Table 5**), in addition to copy number changes that were not resolved by karyotype. The R332 sample was comprised of four highly complex CK subclones (CK1-4) (**Supplementary Figure 4A**), while in the RO20518 sample we also detected ancestral clones with isolated loss of 5q and 15p. To determine if the aneuploidy signature in our iPSC model was shared with AML-CK patients, we generated a module score based on 116 genes upregulated in the +10q/add(21p) clone as the iPSC-Complex Karyotype signature (i-CK) (**Supplementary Figure 4B**). The i-CK signature was upregulated in all R332 CK1-4 clones and some of the RO20518 clones over normal copy number cells identified by CNI in each patient (**Figure 4C**). No chr. 10q gain was detected by CNI or conventional karyotyping in either patient, suggesting that i-CK is a generalizable signature induced in aneuploid HSPCs in AML-CK irrespective of specific abnormalities. *PTEN* and cohesin component *WAPL* were consistently upregulated in aneuploid clones in AML-CK patients (**Figure 4D-E**). *BCL2* was upregulated in R332, but not RO20518 which expressed *CD14* (**Figure 4D-E**), consistent with low expression of *BCL2* in myelo-monocytic AML[41]. To characterize the aneuploidy signature across larger patient cohorts, we analyzed single cell RNAseq data from 5 AML-CK patients reported by Wang et al[42], 8 AML-CK patients reported by Leppa et al[14], and 1 AML-CK patient from Petti et al[43,44]. The samples included those with *TP53* mutation, TP53^{mut} with 17p/-17, and TP53 WT cases, with multiple cytogenetic abnormalities detected by single cell CNI (**Supplementary Figure 4C; Supplementary Table 5**). All 5 patients from Wang et al[42] showed significant enrichment of the i-CK signature, including *PTEN* and cohesins, in complex subclones compared to euploid cells from the same patient (**Figure 4F,G**). Of the 8 patients from Leppä et al[14], 7 showed significant i-CK signature enrichment compared to normal immune cells from the same patient (**Supplementary Figure 4D**). Similarly, i-CK signature was upregulated in the AML-CK patient from Petti et al[43,44] (**Supplementary Figure 5A-C**), but not in patients with del(5q) MDS without complex karyotype (**Supplementary Figure 5D-F**). Taken together, the i-CK signature was broadly upregulated in 14 of 16 AML-CK patients with diverse mutational status and cytogenetic abnormalities. The i-CK signature was also largely distinct from the leukemic stem cell (LSC-17)

signature, which was not positively enriched in aneuploid clones (**Supplementary Figure 5G**). We propose that a generalized gene expression state is associated with aneuploidy in AML-CK, despite different acquired chromosomal abnormalities.

BCL2 is a targetable molecular dependency of aneuploid clones

The anti-apoptotic factor *BCL2,* upregulated in aneuploid HSPCs (**Figure 3D**), is the target of venetoclax, a BCL2 inhibitor clinically used to treat high-risk AML[45-47]. We sought to determine whether aneuploid clones are sensitized to venetoclax and how evolution to aneuploidy is impacted by venetoclax treatment. Venetoclax response can be modulated by the levels of BCL2, other anti-apoptotic BCL2 family proteins, and pro-apoptotic factors (such as BAX)[47,48]. *TP53^{mut}*del5q and the aneuploid +10q/add(21p) HSPCs selectively upregulated *BCL2* (**Figure 3D**), but not other anti-apoptotic paralogs *MCL1*, *BCL2L1*, or *BCL2A1* (**Figure 5A**). Consistent with this, parental *TP53^{mut}*del5q HSPCs were highly sensitive to venetoclax compared to *TP53^{mut}* HSPCs (IC50 ~0.250 μM vs. ~40 μM) (**Figure 5B**). To test how treatment with venetoclax impacts evolution to aneuploidy, we evolved cryopreserved *TP53^{mut}*del5q HSPCs (**Figure 2A**) with continuous treatment with vehicle control or venetoclax at the 250 nM IC50 dose (**Figure 5C**). In the vehicle-treated culture, the same add(21p) [del(5q),add(21p),add(11p)] clone gained relative dominance as in the original experiment, though interestingly it underwent whole genome duplication event to give rise to a 4N subclone (**Figure 5D**, left). In marked contrast, the *BCL2*-high add(21p) clone was eradicated in the venetoclax-treated culture, and instead the del(1p) [del(1p),dup2,del(5q),−21] minor clone became dominant (**Figure 5D**, right). The del(1p) founder clone massively diversified under venetoclax selection into several complex subclones, which gained dic(11;19) and -16 (**Figure 5D**, right). Venetoclax-treated culture displayed a marked resistance to venetoclax (IC50 ~ 70 μM) compared to the vehicle-treated culture with dominant add(21p) clone, which had even greater sensitivity to venetoclax (IC50 ~ 0.02 μM) than the parental *TP53^{mut}*del5q HSPCs (IC50 = 0.25 μM) (**Figure 5E**). These data show that some aneuploid clones are sensitized to venetoclax, with therapy resistance driven by subclonal diversity.

Venetoclax-resistant aneuploid HSPCs undergo a lineage switch

To understand the mechanisms driving venetoclax resistance in AML-CK, we next performed single cell karyotyping. This analysis readily detected the add(21p)/10q+ and the del(1p) clone harboring dup2 and -21 (**Figure 5F**). Venetoclax almost entirely eradicated add(21p)/10q+ and parental *TP53^{mut}*del5q clones, with the culture largely comprised of the del(1p) clone (**Figure 5G; Supplementary Figure 6A,B**). Interestingly, the venetoclax-resistant culture markedly downregulated *BCL2* and upregulated *BCL2A1* expression by qPCR (**Figure 6A**). Single cell analysis showed that *BCL2* expression was reduced in the del(1p) clone in both vehicle- and venetoclax-treated cultures (**Figure 6B**), suggesting that this shift is an intrinsic property of this aneuploid genotype rather than a response to venetoclax. Since HSPC

populations express different levels of BCL2 factors, we next investigated the HSPC composition. The add(21p) clone was largely similar to immature lymphoid-primed multipotent progenitors (LMPP-like). By contrast, the del(1p) clone showed a significant contribution from more mature erythroid-megakaryocyte progenitors (MEP-like) (**Figure 6C, Supplementary Table 6**). Megakaryocyte and erythroid genes were induced in the GO annotation of del(1p)-upregulated genes (**Figure 6D**), including *FLI1*, *TAL1*, *ITGA2B* (CD41) (**Supplementary Figure 6C**), and interestingly JAK/STAT genes *STAT1*, *STAT3*, and *STAT5B* (**Figure 6E**, **Supplementary Table 7)**. Importantly, the gene signature from the MEP-like del(1p) clone was enriched in a subset of AML-CK patients, for example RO20518 that expressed low *BCL2* and was not highly enriched for the i-CK signature (**Supplementary Figure 6D,E**). The patient cohort from Leppä et al[14] included an AML-CK patient (P9) treated with venetoclax. The diagnostic sample was comprised of a dominant CK3 clone which expressed high i-CK signature/*BCL2* and immature markers (CD34, CD117), and a minor clone CK1 which expressed low i-CK signature/*BCL2* and MEP markers (CD71, CD41) (**Supplementary Figure 6F-I**). Consistent with our model, venetoclax treatment depleted the immature CK3 clone leading to clonal dominance of the MEP-like CK1 clone **(Supplementary Figure 6H)**. These data suggest that venetoclax-resistant aneuploid clones can undergo a lineage switch from a more primitive to an MEP-like progenitor cell identity that intrinsically express lower levels of *BCL2*.

Since aneuploid MEP-like HSPCs may be sensitized to distinct drug classes, we screened the parental, vehicle- and venetoclax-treated lines with a panel of FDA-approved drugs for hematological malignancies (**Supplementary Figure 7A**, **Supplementary Table 8**). Interestingly, venetoclax-resistant HSPCs with dominant del(1p) clone were sensitized to multiple JAK2 inhibitors clinically used to treat myeloproliferative neoplasms, including ruxolitinib, momelotinib, fedratinib, and pacritinib (**Supplementary Figure 7B)**. We further validated that venetoclax-resistant HSPCs were sensitized to ruxolitinib compared to vehicle-treated cells (**Figure 6F**). To test the combination of venetoclax and JAK2 inhibitor, we treated aneuploid HSPCs with venetoclax as before (Figure 5C), allowing outgrowth of resistant clones, followed by treatment with ruxolitinib. Ruxolitinib at the IC50 dose of 50 nM suppressed the outgrowth of the venetoclax-resistant MEP-like del(1p) clone by ~2.5 fold (**Figure 6G-I**). Lastly, we tested venetoclax and JAK2 inhibitors in three primary AML-CK samples. Two of these samples had poor response to venetoclax alone (IC50 >2 μM; **Supplementary Figure 7C)**, but were resensitized in combination with JAK2 inhibitor, especially pacritinib (**Supplementary Figure 7D**). Taken together, we show that venetoclax monotherapy resistance can arise from aneuploid HSPCs with MEP-like lineage identity that are sensitized to distinct drug classes.

Discussion

The clonal origins of myeloid neoplasms with complex karyotype remain largely unknown. Here, we develop an iPSC model system in which preleukemic HSPCs evolve to complex and diverse aneuploid states following transient mitotic inhibition. Using this model, we demonstrate that iPSC-derived AML-CK preleukemic HSPCs with *TP53* mutation and del(5q), but not *TP53* mutation alone, undergo complex karyotype evolution marked by sequential acquisition of chromosomal abnormalities. By tracking this process at single cell resolution, we identify a gene expression signature shared with AML-CK patients. We propose that despite distinct collections of chromosome abnormalities, aneuploidy in AML-CK is associated with generalized gene expression states, reflecting the clonal origin and molecular dependencies of aneuploidy, such as anti-apoptotic BCL2 factors. Aneuploid clones were sensitized to standard of care venetoclax therapy, with resistance driven by lineage switching to HSPC states with low *BCL2* expression. These findings show the existence of molecular dependences in aneuploid HSPCs which can be therapeutically targeted in *TP53*-mutant leukemias.

AML-CK presents with widespread aneuploidy at diagnosis making it difficult to reconstruct clonal origins. Near-complete penetrance of *TP53* mutations and their detection in clonal hematopoiesis and in preleukemic clones from AML-CK patients[10,11] suggests that these are initiating mutations. Most patients with AML-CK harbor recurrent deletions on chromosome 5q, suggesting that this region encodes critical genes that cooperate with mutant *TP53* to drive AML-CK progression[7,17-19]. Here, we provide the first experimental evidence that 5q loss is a driver of AML-CK progression. Loss of 5q is also an early event in myeloid oncogenesis, and isolated del(5q) defines a subtype of MDS with favorable prognosis and macrocytic anemia[19], which can progress to high-risk MDS/AML via secondary mutations, including in *TP53*[49]. This suggests that del(5q) may be the initiating lesion in some patients followed by secondary *TP53* mutations. The commonly deleted 5q region in AML-CK spans 5q22-q31 which encodes multiple genes implicated in disease pathogenesis, including *EGR1, APC, CDC25C, CTNNA1,* and *LMNB1*[20-23]. The identification of 5q tumor suppressor genes with roles in regulating genome stability remains an important goal. We propose a common origin of AML-CK that requires cooperative genetic loss of *TP53* and del(5q) and inhibition of mitotic checkpoint integrity via genotoxic or cytotoxic therapy.

Clonal trajectories of chromosomal evolution in the human hematopoietic system have not been studied experimentally. Chromosomal shattering, termed chromothripsis, is observed in genetically unstable tumors suggestive of a rapid, catastrophic evolution[3,50]. Evolution in our model is consistent with a more gradualist model of neoplastic progression, in which rare aneuploid cells arising after mitotic checkpoint inhibition diversify in a sequential fashion. Other studies of *TP53*-mutated secondary AML are also suggestive of a sequential model of aneuploidy[51]. Recent single cell analysis in AML-CK patients has uncovered evidence for both sequential and punctuated evolution[14], although detection of early clones remains rare.

By using single cell CNI to track this evolutionary process, we identify an i-CK gene expression signature shared with AML-CK patients. This signature is marked by upregulation of HSC genes and genome integrity factors including *PTEN*[40] and cohesin subunits, including *SMC3* and *WAPL*. Aneuploidy imposes unique cellular stresses on proteostasis, replication, and mitosis[24]. Inappropriate chromatid pairing during mitosis induces high levels of genome instability that can be incompatible with cell survival[52]. Interestingly, PTEN has a non-canonical role in promoting genome integrity in mitosis[39]. Cohesins mediate chromosome pairing in early mitosis and cohesin cleavage is required for anaphase progression. Critically, while cohesin mutations in *STAG2* portend a poor prognosis in myeloid neoplasms, they are mutually exclusive with *TP53* mutations and are almost never observed in AML-CK[53]. We hypothesize that upregulation of PTEN and cohesins enables aneuploid cells to stabilize chromosome pairing in mitosis, explaining why diverse CK genotypes converge on this i-CK signature. Our model of AML-CK will enable further dissection of the mechanisms required for the maintenance of an aneuploid cell state in HSPCs.

TP53 mutation and complex karyotype defines a high-risk subgroup of myeloid neoplasms with poor response to antileukemic therapies[17,25], including BCL2 inhibitor venetoclax[45,54-56]. We find that *BCL2* is often upregulated as part of the i-CK signature and may promote the survival of aneuploid clones. Treatment with venetoclax eradicates clones expressing high *BCL2* levels, however, resistance is driven by aneuploid clones with reduced expression of BCL2 and induction of alternative BCL2 family factors, such as BCL2L1 and BCL2A1. The switch to alternative BCL2 factors characterizes normal hematopoietic differentiation; BCL2 expression declines during myeloid differentiation with dependence on MCL1[41], whereas erythroid and megakaryocyte lineages are dependent on BCL2L1[57]. Interestingly, AMLs in which LSCs display expression of mature monocytic or erythroid/megakaryocyte programs display poor responses to venetoclax[41,48,57]. Consistent with this, our data suggests that venetoclax-resistant aneuploid clones undergo an erythroid/megakaryocyte lineage switch which sensitizes them to JAK2 inhibition. We propose that similarly to non-aneuploid leukemias, LSCs in AML-CK likely exist in a spectrum of cell states from more primitive (HSC-like) to more mature (MEP-like) among diverse clones, with distinct molecular vulnerabilities[58]. More broadly, we propose that aneuploid cell states confer unique molecular vulnerabilities which can be therapeutically targeted in high-risk *TP53*-mutant leukemias.

Acknowledgements

The authors would like to thank Columbia University Irving Medical Center Clinical Cytogenetics Laboratory, Diagnostic Cytogenetics (DCI), and Fred Hutchinson Clinical Cancer Genomics for providing cytogenetics services. Kate Kroeger and Krysta Starr for assistance with cytogenetics. Tim Monahan, Sioban B. Keel, Derek Stirewalt, and the Fred Hutch/University of Washington Leukemia Repository and Mayo Clinic Biorepository for Acute Leukemia Research for clinical samples. Tim Martins at the ISCRM Quellos High-Throughput Screening Core, Aurelio Silverstroni (Pathology Flow Core) for technical assistance, and Douglas M. Fowler for feedback on the study. J.P.C. is supported by the NHLBI training grant T32HL007093-50. S.D. is supported by the grants from National Heart, Lung, and Blood Institute (R01 HL151651 and R01 HL169156), NIDDK (RC2-DK127989), and Edward P. Evans Foundation. S.D. is a Scholar of the Blood Cancer United Society (1391-24). P.S.B. is also supported by NIDDK (RC2-DK127989). E.M.S and S.D. are supported by R01 CA272594. A.N.S. is a Robert Winn Diversity in Clinical Trials Scholar. S.H.K. and A.N.S. are supported by R01 CA289285.

Author Contributions

J.P.C., and S.D. conceived the project and designed the experiments; J.P.C., performed the experiments with help from S.R., S.S., V.J., and J.W.; J.P.C., S.R., S.G., F.Y.H., AM.L., V.J., P.S.B, A.T., M.F., E.M.S., and S.D., analyzed and interpreted the data; J.L.A., J.S.A., S.H.K., P.S.B, A.T., V.J., M.F., and E.M.S., provided input on experimental design and interpretation. B.W., and H.A.A. provided patient sample data. A.N.S., S.H.K., J.S.A., J.L.A., and E.M.S., provided patient samples and clinical interpretation; J.P.C., and S.D. prepared the manuscript.

Competing Interests

H.A.A. received honorarium and in-kind support from Illumina. The other authors declare no potential conflicts of interest.

References

1. Sansregret L, Swanton C. The Role of Aneuploidy in Cancer Evolution. *Cold Spring Harb Perspect Med*. 2017;7(1).
2. Ben-David U, Amon A. Context is everything: aneuploidy in cancer. *Nature Reviews Genetics*. 2020;21(1):44-62.
3. Santaguida S, Amon A. Short- and long-term effects of chromosome mis-segregation and aneuploidy. *Nature Reviews Molecular Cell Biology*. 2015;16(8):473-485.
4. Bakhoum SF, Cantley LC. The multifaceted role of chromosomal instability in cancer and its microenvironment. *Cell*. 2018;174(6):1347-1360.
5. Khoury JD, Solary E, Abla O, et al. The 5th edition of the World Health Organization Classification of Haematolymphoid Tumours: Myeloid and Histiocytic/Dendritic Neoplasms. *Leukemia*. 2022;36(7):1703-1719.
6. Leung GMK, Zhang C, Ng NKL, et al. Distinct mutation spectrum, clinical outcome and therapeutic responses of typical complex/monosomy karyotype acute myeloid leukemia carrying TP53 mutations. *Am J Hematol*. 2019;94(6):650-657.
7. Rucker FG, Schlenk RF, Bullinger L, et al. TP53 alterations in acute myeloid leukemia with complex karyotype correlate with specific copy number alterations, monosomal karyotype, and dismal outcome. *Blood*. 2012;119(9):2114-2121.
8. Daneshbod Y, Kohan L, Taghadosi V, Weinberg OK, Arber DA. Prognostic Significance of Complex Karyotypes in Acute Myeloid Leukemia. *Curr Treat Options Oncol*. 2019;20(2):15.
9. McNerney ME, Godley LA, Le Beau MM. Therapy-related myeloid neoplasms: when genetics and environment collide. *Nature Reviews Cancer*. 2017;17(9):513-527.
10. Wong TN, Ramsingh G, Young AL, et al. Role of TP53 mutations in the origin and evolution of therapy-related acute myeloid leukaemia. *Nature*. 2015;518(7540):552-555.
11. Kwan TT, Oza AM, Tinker AV, et al. Preexisting TP53-Variant Clonal Hematopoiesis and Risk of Secondary Myeloid Neoplasms in Patients With High-grade Ovarian Cancer Treated With Rucaparib. *JAMA Oncol*. 2021;7(12):1772-1781.
12. Jaiswal S, Fontanillas P, Flannick J, et al. Age-related clonal hematopoiesis associated with adverse outcomes. *N Engl J Med*. 2014;371(26):2488-2498.
13. Weeks LD, Niroula A, Neuberg D, et al. Prediction of Risk for Myeloid Malignancy in Clonal Hematopoiesis. *NEJM Evidence*. 2023;2(5):EVIDoa2200310.
14. Leppa AM, Grimes K, Jeong H, et al. Single-cell multiomics analysis reveals dynamic clonal evolution and targetable phenotypes in acute myeloid leukemia with complex karyotype. *Nat Genet*. 2024;56(12):2790-2803.
15. Zhakula-Kostadinova N, Taylor AM. Patterns of Aneuploidy and Signaling Consequences in Cancer. *Cancer Res*. 2024;84(16):2575-2587.
16. Shih J, Sarmashghi S, Zhakula-Kostadinova N, et al. Cancer aneuploidies are shaped primarily by effects on tumour fitness. *Nature*. 2023;619(7971):793-800.
17. Mrózek K, Eisfeld A-K, Kohlschmidt J, et al. Complex karyotype in de novo acute myeloid leukemia: typical and atypical subtypes differ molecularly and clinically. *Leukemia*. 2019;33(7):1620-1634.
18. Mrozek K. Cytogenetic, molecular genetic, and clinical characteristics of acute myeloid leukemia with a complex karyotype. *Semin Oncol*. 2008;35(4):365-377.
19. Ebert BL. Deletion 5q in myelodysplastic syndrome: a paradigm for the study of hemizygous deletions in cancer. *Leukemia*. 2009;23(7):1252-1256.
20. Reilly A, Philip Creamer J, Stewart S, et al. Lamin B1 deletion in myeloid neoplasms causes nuclear anomaly and altered hematopoietic stem cell function. *Cell Stem Cell*. 2022;29(4):577-592 e578.
21. Stoddart A, Fernald AA, Wang J, et al. Haploinsufficiency of del(5q) genes, Egr1 and Apc, cooperate with Tp53 loss to induce acute myeloid leukemia in mice. *Blood*. 2014;123(7):1069-1078.
22. Wei S, Chen X, Rocha K, et al. A critical role for phosphatase haplodeficiency in the selective suppression of deletion 5q MDS by lenalidomide. *Proc Natl Acad Sci U S A*. 2009;106(31):12974-12979.

23. Liu TX, Becker MW, Jelinek J, et al. Chromosome 5q deletion and epigenetic suppression of the gene encoding alpha-catenin (CTNNA1) in myeloid cell transformation. *Nat Med*. 2007;13(1):78-83.
24. Zhu J, Tsai HJ, Gordon MR, Li R. Cellular Stress Associated with Aneuploidy. *Dev Cell*. 2018;44(4):420-431.
25. Daver NG, Maiti A, Kadia TM, et al. TP53-Mutated Myelodysplastic Syndrome and Acute Myeloid Leukemia: Biology, Current Therapy, and Future Directions. *Cancer Discov*. 2022;12(11):2516-2529.
26. Hsu J, Reilly A, Hayes BJ, et al. Reprogramming identifies functionally distinct stages of clonal evolution in myelodysplastic syndromes. *Blood*. 2019;134(2):186-198.
27. Doulatov S, Vo LT, Chou SS, et al. Induction of multipotential hematopoietic progenitors from human pluripotent stem cells via respecification of lineage-restricted precursors. *Cell Stem Cell*. 2013;13(4):459-470.
28. Stuart T, Butler A, Hoffman P, et al. Comprehensive integration of single-cell data. 2019;177(7):1888-1902. e1821.
29. Gao T, Soldatov R, Sarkar H, et al. Haplotype-aware analysis of somatic copy number variations from single-cell transcriptomes. *Nat Biotechnol*. 2023;41(3):417-426.
30. Devillers R, Dos Santos A, Destombes Q, Laplante M, Elowe S. Recent insights into the causes and consequences of chromosome mis-segregation. *Oncogene*. 2024;43(43):3139-3150.
31. Colombo R, Caldarelli M, Mennecozzi M, et al. Targeting the Mitotic Checkpoint for Cancer Therapy with NMS-P715, an Inhibitor of MPS1 Kinase. *Cancer Research*. 2010;70(24):10255-10264.
32. Klaasen SJ, Truong MA, van Jaarsveld RH, et al. Nuclear chromosome locations dictate segregation error frequencies. *Nature*. 2022;607(7919):604-609.
33. Lambuta RA, Nanni L, Liu Y, et al. Whole-genome doubling drives oncogenic loss of chromatin segregation. *Nature*. 2023;615(7954):925-933.
34. Salehi S, Kabeer F, Ceglia N, et al. Clonal fitness inferred from time-series modelling of single-cell cancer genomes. *Nature*. 2021;595(7868):585-590.
35. Tenaillon O, Barrick JE, Ribeck N, et al. Tempo and mode of genome evolution in a 50,000-generation experiment. *Nature*. 2016;536(7615):165-170.
36. Good BH, McDonald MJ, Barrick JE, Lenski RE, Desai MM. The dynamics of molecular evolution over 60,000 generations. *Nature*. 2017;551(7678):45-50.
37. Gao R, Bai S, Henderson YC, et al. Delineating copy number and clonal substructure in human tumors from single-cell transcriptomes. *Nature Biotechnology*. 2021;39(5):599-608.
38. Hao Y, Hao S, Andersen-Nissen E, et al. Integrated analysis of multimodal single-cell data. *Cell*. 2021;184(13):3573-3587.e3529.
39. Shen WH, Balajee AS, Wang J, et al. Essential role for nuclear PTEN in maintaining chromosomal integrity. *Cell*. 2007;128(1):157-170.
40. Yilmaz OH, Valdez R, Theisen BK, et al. Pten dependence distinguishes haematopoietic stem cells from leukaemia-initiating cells. *Nature*. 2006;441(7092):475-482.
41. Pei S, Pollyea DA, Gustafson A, et al. Monocytic Subclones Confer Resistance to Venetoclax-Based Therapy in Patients with Acute Myeloid Leukemia. *Cancer Discov*. 2020;10(4):536-551.
42. Wang B, Reville PK, Yassouf MY, et al. Comprehensive characterization of IFNgamma signaling in acute myeloid leukemia reveals prognostic and therapeutic strategies. *Nat Commun*. 2024;15(1):1821.
43. Petti AA, Williams SR, Miller CA, et al. A general approach for detecting expressed mutations in AML cells using single cell RNA-sequencing. *Nature Communications*. 2019;10(1):3660.
44. Klco JM, Spencer DH, Miller CA, et al. Functional heterogeneity of genetically defined subclones in acute myeloid leukemia. *Cancer Cell*. 2014;25(3):379-392.
45. DiNardo CD, Jonas BA, Pullarkat V, et al. Azacitidine and Venetoclax in Previously Untreated Acute Myeloid Leukemia. *New England Journal of Medicine*. 2020;383(7):617-629.
46. Roberts AW, Wei AH, Huang DCS. BCL2 and MCL1 inhibitors for hematologic malignancies. *Blood*. 2021;138(13):1120-1136.
47. Konopleva M, Pollyea DA, Potluri J, et al. Efficacy and Biological Correlates of Response in a Phase II Study of Venetoclax Monotherapy in Patients with Acute Myelogenous Leukemia. *Cancer Discov*. 2016;6(10):1106-1117.

48. Waclawiczek A, Leppa AM, Renders S, et al. Combinatorial BCL2 Family Expression in Acute Myeloid Leukemia Stem Cells Predicts Clinical Response to Azacitidine/Venetoclax. *Cancer Discov*. 2023;13(6):1408-1427.
49. Montoro MJ, Palomo L, Haferlach C, et al. Influence of TP53 gene mutations and their allelic status in myelodysplastic syndromes with isolated 5q deletion. *Blood*. 2024;144(16):1722-1731.
50. Rucker FG, Dolnik A, Blatte TJ, et al. Chromothripsis is linked to TP53 alteration, cell cycle impairment, and dismal outcome in acute myeloid leukemia with complex karyotype. *Haematologica*. 2018;103(1):e17-e20.
51. Rodriguez-Meira A, Norfo R, Wen S, et al. Single-cell multi-omics identifies chronic inflammation as a driver of TP53-mutant leukemic evolution. *Nat Genet*. 2023;55(9):1531-1541.
52. Passerini V, Ozeri-Galai E, de Pagter MS, et al. The presence of extra chromosomes leads to genomic instability. *Nat Commun*. 2016;7:10754.
53. Gao J, Aksoy BA, Dogrusoz U, et al. Integrative Analysis of Complex Cancer Genomics and Clinical Profiles Using the cBioPortal. *Science Signaling*. 2013;6(269):pl1-pl1.
54. Shah MV, Chhetri R, Dholakia R, et al. Outcomes following venetoclax-based treatment in therapy-related myeloid neoplasms. *Am J Hematol*. 2022;97(8):1013-1022.
55. Kim K, Maiti A, Loghavi S, et al. Outcomes of TP53-mutant acute myeloid leukemia with decitabine and venetoclax. *Cancer*. 2021;127(20):3772-3781.
56. Daver NG, Iqbal S, Renard C, et al. Treatment outcomes for newly diagnosed, treatment-naïve TP53-mutated acute myeloid leukemia: a systematic review and meta-analysis. *Journal of Hematology & Oncology*. 2023;16(1):19.
57. Kuusanmaki H, Dufva O, Vaha-Koskela M, et al. Erythroid/megakaryocytic differentiation confers BCL-XL dependency and venetoclax resistance in acute myeloid leukemia. *Blood*. 2023;141(13):1610-1625.
58. Waclawiczek A, Leppa AM, Renders S, Trumpp A. An arms-race against resistance: leukemic stem cells and lineage plasticity. *Mol Oncol*. 2024;18(3):475-478.

586 **Table 1**

Exp	Gen	Sample	Treat	Days	% Aneupl.	Karyotype
1	Pooled	1A	NMS	38	57	46,XX,del(5)(q22q31)[16]/46,idem,add(2)(p13)[16]/48,idem,+8,+20[5]/46,XX[3] (6/16 del5q non-clonal)
2	TP53	P53-2A	NMS	35	0	46,XX[30] (3 non-clonal)
2	TP53	P53-2A	NMS	76	10	47,XX,+8[2]/46,XX[18] (3/18 non-clonal)
2	del5q	del5q-2A	NMS	35	33	46,XX,del(5)(q22q31)[20]/47,sl,+10[4]/45,sl,-21[3]/46,sl,add(21)(p11.2)[3]
2	del5q	del5q-2A	NMS	76	100	46,XX,del(5)(q22q31),add(21)(p12)[12]/46,idem,add(11)(p15)[8]
2	TP53	P53-2A (rethaw)	NMS	57	0	46,XX[22] (4/22 non-clonal)
2	del5q	del5q-2A (rethaw)	NMS	57	100	45,XX,del(5)(q15q31),del(1)(p36.1p?32),dup(2)(q21q31),-21[18]/46,XX,del(5)(q15q31),add(21)(p 11.2)[2]
3	TP53	P53-3control	DMSO	60	15	46,XX,dup(1)(q21q32)[3]/46,XX[17] (2 non-clonal)*
3	TP53	P53-3A	NMS	38	10	46,XX,dup(1)(q21q32)[2]/48,XX,+10,+19[2]/46,XX[16] (2 non-clonal)*
3	TP53	P53-3B	NMS	38	0	46,XX,dup(1)(q21q32)[2]/46,XX[18] (2 non-clonal +3/+6)*
3	TP53	P53-3C	NMS	38	0	46,XX,dup(1)(q21q32)[3]/46,XX[17] (2 non-clonal -15/-17)*
3	TP53	P53-3D	NMS	38	0	46,XX,dup(1)(q21q32)[6]/46,XX[14] (3/14 non-clonal -8-13/-5-14-15/+1+7)*
3	TP53	P53-3A	NMS	72	10	46,XX,dup(1)(q21q32)[2]/46,XX,+del(1)(p13),-17[2]/46,XX[16]*
3	TP53	P53-3B	NMS	72	0	46,XX,dup(1)(q21q32)[3]/46,XX[17]*
3	TP53	P53-3C	NMS	72	15	46,XX,dup(1)(q21q32)[2]/46,XX,+1,add(1)(p12),del(1)(q12),-17[3]/46,XX[15]*
3	TP53	P53-3D	NMS	72	0	46,XX,dup(1)(q21q32)[4]/46,XX[16]*
3	del5q	del5q-3control	DMSO	60	0	46,XX,del(5)(q22q33)[20]
3	del5q	del5q-3A	NMS	38	10	46,XX,del(5)(q22q31)[18]/45,XX,sl,-15[2] (4 non-clonal -19/-20/-11-18/+8-19)
3	del5q	del5q-3B	NMS	38	30	46,XX,del(5)(q22q31)[14]/45,sl,dic(11;19)(p15;q13.3)[3]/47,sl,+10[2]/47,sl,+8[1]
3	del5q	del5q-3C	NMS	38	40	46,XX,del(5)(q22q31)[12]/47,idem,+8[8] (3 non-clonal -10/-18/-21)
3	del5q	del5q-3D	NMS	38	45	46,XX,del(5)(q22q31)[11]/47,idem,+8[8]/47,idem,+10[1] (3 non-clonal -11/-13/-16)
3	del5q	del5q-3A+B+C+D	NMS	57	90	46,XX,del(5)(q22q33)[2]/47,XX,del(5),+8[15]/48,XX,del(5),+8,+10[4] (7 non-clonal, in +8 samples?)
3	del5q	del5q-3A	NMS	72	90	46,XX,del(5)(q22q33)[2]/47,XX,del(5)(q22q33),+8[12]/47,XX,del(5)(q22q33),+10[1]/47,XX,del(5)(q22q33),+8,add(11)(p15)[4]/47,XX,del(5),+10,add(11)(p15),add(19)(q13.4[1]
3	del5q	del5q-3B	NMS	72	95	46,XX,del(5)(q22q33)[1]/47,XX,del(5)(q22q33),+8[6]/48,XX,del(5)(q22q33),+8,+10[2]/48,XX,del(5)(q22q33),+8,+19[6]/47,XX,del(5)(q22q33),+8,add(11)(p15)[2]/ 47,XX,del(5)(q22q33),+10,add(11)(p15)[1]/47,XX,del(5)(q22q33),+8,add(19)(q13.4)[2]/45,XX,del(5),+8,add(11)(p15),-19[1]
3	del5q	del5q-3C	NMS	72	90	46,XX,del(5)(q22q33)[2]/47,XX,del(5)(q22q33),+8[13]/47,XX,del(5)(q22q33),+10[1]/48,XX,del(5)(q22q33),+8,+10[3]/47,XX,del(5)(q22q33),+8,add(11)(p15),add(19)(q13.4)[1]
3	del5q	del5q-3D	NMS	72	100	47,XX,del(5)(q22q33),+8[11]/47,XX,del(5)(q22q33),+10[4]/48,XX,del(5)(q22q33),+8.+10[3]/48,XX,del(5)(q22q33),+8, add(11)(p15)[2]
4	TP53	P53-4control	DMSO	38	0	46,XX[20]
4	TP53	P53-4A	NMS	38	0	46,XX[20]
4	del5q	del5q-4control	DMSO	38	15	46,XX,del(5)(q22q31)[17]/46,XX,del(5)(q22q31),dic(11;19)(p15;q13.3)[3]
4	del5q	del5q-4A	NMS	38	45	46,XX,del(5)(q22q31)[11]/47,XX,del(5)(q22q31),+8[7]/47,XX,del(5)(q22q31),+10[2]

Table 1. Karyotypes of HSPC evolution to aneuploidy experiments. Complete karyotype reports of *TP53*^{mut}and *TP53*^{mut}del5qHSPC experiments after treatment with NMS-P715 or DMSO vehicle control shown in Figure 1B and Figure 1E. Columns are organized as follows: experiment (Exp) 1-4; genotype (Gen): TP53 = *TP53*^{mut}, del5q = *TP53*^{mut}del5q; sample name (A,B,C, etc.); treatment (NMS or DMSO control); days: culture period after NMS treatment when karyotype was determined; % Aneupl.: percentage of cells with altered karyotype from the parental line. New abnormalities detected in TP53^{mut} HSPCs are shown in blue font. New abnormalities detected in *TP53*^{mut}del5q HPSCs are shown in red font. Experiment #3 corresponds to the parallel evolution experiment in Figure 2D in which sub-cultures A,B,C,D were split from the same primary culture. In experiment #3, a spontaneous dup(1)(q21q32) abnormality was observed in *TP53*^{mut} DMSO control cultures, and clones with this abnormality (marked with *) were not included in the calculated percentage of aneuploid cells for NMS-treated cultures from the same original culture.

Figure Legends

Figure 1. Experimental model of aneuploid evolution in *TP53*-mutant preleukemic HSPCs. (A) Schematic of reprogramming of *TP53*^{mut} and *TP53*^{mut}del5q iPSCs from a patient with MDS/AML-CK and differentiation into iPSC-HSPCs. Cells were exposed to 1 μM MPS1 inhibitor NMS-P715 for 24 hours, washed, and cultured continuously for 5-10 weeks. Cytogenetic analysis was performed using conventional karyotyping to analyze clonal dynamics of aneuploid cells. **(B)** Percentage of aneuploid cells over time post NMS-P715 treatment as reported by karyotyping (left), and a representative aneuploid clone with trisomy 8 and 20 evolved from *TP53*^{mut}del5q HSPCs. Connected line indicates measurements over time in the same culture (n = 7 independent cultures derived from n = 3 NMS-P715 treated samples). **(C)** Number of chromosome abnormalities per clone compared to parental lines (karyotype complexity); n=8 independent cultures derived from n = 4 NMS-P715 treated samples, two tailed Mann Whitney Test (***p=0.002). **(D)** Number of distinct aneuploid clones detected by karyotyping in each culture; n = 8 independent experiments, two-tailed Mann Whitney Test (****p<0.0001). **(E)** Summary of chromosome abnormalities identified by karyotyping in aneuploid clones derived from *TP53*^{mut}del5q HSPCs. Each row is a separate clone with experiments grouped by color (n = 18 clones derived from n = 4 NMS-P715 treated samples), individual chromosomes are in columns, and chromosome rearrangements are shown in color: red = amplification, blue = hemizygous deletion, purple = unknown material/rearrangement. Detailed information is included in Table 1.

Figure 2. Evolution of aneuploidy is a stepwise process shaped by clonal competition. (A) Experimental scheme of HSPC evolution to aneuploidy following 24-hour NMS-P715 MPSi treatment. A portion of the culture was cryopreserved, thawed, and compared to the primary culture. **(B)** Clonal dynamics fish plot of a *TP53*^{mut}del5q evolution experiment, with primary experiment (top plot) and repeat experiment from cryopreserved sample (bottom plot). The proportion of each clone over time is shown as determined by manual karyotyping at time points indicated by hashed lines. Individual clones are shown in colors with inferred lineage indicated. **(C)** Mean relative fitness (s + 1) of each clone in the primary vs. cryopreserved cultures in (B); mean and 1-99th percentile of 9000 replicates. Dotted line indicates neutral fitness. **(D)** Experimental scheme of the parallel culture experiment, in which *TP53*^{mut} or *TP53*^{mut}del5q HSPCs were split into 4 separate cultures (A,B,C,D) immediately after 24-hour NMS-P715 MPSi treatment, cultured in parallel, and analyzed by karyotyping at time points indicated by hashed lines. **(E)** Clonal dynamics fish plots of the parallel A,B,C,D cultures showing the proportion of each clone determined by manual karyotyping. Clones are shown in colors with inferred lineage indicated. **(F)** Mean relative fitness (s + 1) for each clone in parallel cultures in (D). Neutral fitness (1+s = 1) is shown with dotted line. Each point is a mean of 9000 replicates for each culture, bars indicate mean of means ± S.D.

Figure 3. Single cell analysis identifies gene expression signature of aneuploidy. (A) Experimental scheme of time course experiment. *TP53*^{mut} and *TP53*^{mut}del5q HSPCs were evolved and sequentially sampled by single cell RNAseq at time points indicated, and clonal makeup defined by CNI. **(B)** Clonal dynamic fish plot of the *TP53*^{mut}del5q culture corresponding to Figure 2B determined by single cell CNI using the Numbat package at time points indicated by hashed lines. **(C)** Copy number abnormalities in single cells identified using Numbat; data combined from all timepoints in *TP53*^{mut} and *TP53*^{mut}del5q lines. CNAs are shown in color: red = amplification, blue = deletion, green = copy number-neutral loss of heterozygosity. Clonal identity based on probability that the cell belongs to each inferred clone is shown as color bar on the left: gray = *TP53*^{mut} only, green = *TP53*^{mut}del5q , blue = *TP53*^{mut}del5q+10q. **(D)** Normalized gene expression level in single cell clones identified by Numbat; log scale, black dot indicates mean. **(E)** Top gene ontology categories in Metascape for genes upregulated in aneuploid *TP53*^{mut}del5q+10q compared to parental *TP53*^{mut}del5q HSPCs. Upregulated genes were defined by Wilcoxon Rank Sum Test, $q < 0.05$. Log (q-value) of each term is displayed ($q < 0.05$).

Figure 4. Aneuploidy signature is shared with AML-CK patients. (A) Experimental scheme of single cell transcriptomic analysis comparing *TP53*^{mut}del5q iPSC-HSPCs and patients with AML-CK sequenced in the study, as well as Leppä et al[14], Wang et al[42], and Petti et al[43,44] published datasets. **(B)** Copy number abnormalities identified in single cells of AML-CK patient RO20518. Red = amplification, blue = deletion, green = copy number-neutral loss of heterozygosity. Clonal identity based on probability that the cell belongs to each inferred clone is shown as color bar on the left: grey = WT, orange = del(5q)+del(15p), green/blue = CK clones #1-2. **(C)** Normalized expression of the i-CK signature genes in single cell clones of AML-CK patients RO20518 and R332; log scale, black dot indicates median; statistical testing: R332 all CK clones enriched for i-CK ($p<0.0001$), RO20518 del5q ($p<0.0001$) (Holm Adjusted Wilcox Rank Sum test). **(D)** Normalized gene expression level in single cell clones (WT, del5q, CK1-2) in AML-CK patient RO20518; log scale, black dot indicates median. **(E)** Normalized gene expression level in single cell clones (WT, CK1-4) in AML-CK patient R332; log scale, black dot indicates mean. **(F)** Normalized expression of the i-CK signature genes in single cell aneuploid (CK) or euploid (WT) clones of AML-CK patients from Wang et al[42]; black dot indicates mean; statistical testing: PT6A, PT10A, PT16A, PT27A, PT29A all CK clones enriched for i-CK, $p<0.0001$, Holm Adjusted Wilcox Rank Sum test. **(G)** Normalized gene expression level of *PTEN* and *SMC3* in single cell single cell euploid (WT) or aneuploid (CK) clones in AML-CK patients from Wang et al; log scale.

Figure 5. BCL2 is a targetable molecular dependency of aneuploid clones. (A) Normalized gene expression level in single cell clones identified by Numbat from iPSC HSPCs; log scale, black dot indicates mean. **(B)** Relative cell viability of parental *TP53*^{mut} and *TP53*^{mut}del5q HSPCs treated with venetoclax in dose response format, for 7 days. Concentration plotted as log10 nM. **(C)** Experimental

scheme of venetoclax (VEN) treatment, in which HSPCs harboring the *BCL2*-high del5q+10q subclone (Figure 2B) are evolved with 250 nM VEN or DMSO vehicle for ~48 days and sampled periodically for karyotype. **(D)** Clonal dynamics fish plots of the *TP53*^{mut}del5q cultures evolved in the presence of DMSO vehicle (left) or VEN (right) (day 14-62) showing the proportion of each clone determined by manual karyotyping. Clones are shown in colors with inferred lineage indicated. **(E)** Relative cell viability of *TP53*^{mut}del5q-derived cultures evolved with VEN or DMSO and parental lines treated with VEN in dose response format, for 7 days. Concentration plotted as log10 nM. **(F)** Copy number abnormalities identified by Numbat in single cells of pooled vehicle and venetoclax-treated samples. Red = amplification, blue = deletion, green = copy number-neutral loss of heterozygosity. Clonal identity based on probability that the cell belongs to each inferred clone is shown as color bar on the left: grey/orange = del5q parental, green = add21p/+10q, and blue = del(1p). **(G)** Percent clonal contribution for each culture as determined by Numbat single cell CNI; add21p = [del(5q);add(21p)/+10q], del1p = [del(5q);del(1p);dup(2);-21].

Figure 6. Venetoclax-resistant aneuploid HSPCs undergo a lineage switch. (A) Expression of BCL2 family genes in bulk *TP53*^{mut}del5q HSPCs evolved in the presence of vehicle or venetoclax compared to parental lines. Expression measured relative to *GAPDH* by qPCR and normalized to *TP53*^{mut} HSPCs. **(B)** Violin plots of expression of BCL2 family genes in single cells with clonal identity determined by CNI. Color indicates treatment condition (vehicle or venetoclax), log scale, black dot indicates mean. **(C)** Lineage composition identified by SingleR for add(21p) and del(1p) clones determined by CNI. Cell types with < 5 cells in both conditions were excluded. **(D)** Top gene ontology categories in Metascape analysis on 284 upregulated (LFC > 0.5, Wilcoxon Rank Sum Test q value > 0.05) genes in the del(1p) clone vs the parental *TP53*^{mut}del5q clone. Log (q-value) of each term is displayed (q < 0.05). **(E)** Violin plots of expression of STAT family genes differentially expressed between del(1p) and *TP53*^{mut}del5q parental HSPCs, colored by clone, log scale, black dot indicates mean. **(F)** Normalized relative mean cell viability of aneuploid cultures treated with the JAK2 inhibitor ruxolitinib. *TP53*^{mut}del5q HSPCs evolved in the presence of vehicle or venetoclax and parental lines were treated with ruxolitinib in dose response format for 5 days. n=2, concentration plotted as $\log_{10}$ nM. **(G)** Cell growth of HSPCs from the add(21p)/del(1p) culture (Figure 5C) treated sequentially with venetoclax and JAK2 inhibitor ruxolitinib. HSPCs were treated with 250 nM venetoclax (VEN) or DMSO vehicle (Veh) between day 14 to 35, and subsequently treated with 50 nM ruxolitinib (RUX) or vehicle between day 35 to 49. Left: cell growth of vehicle- or VEN-treated cultures as fold expansion relative to day 14. Right: cell growth of vehicle- or RUX-treated cultures as fold expansion relative to day 35. **(H)** Clonal expansion of venetoclax-untreated cultures treated with vehicle or RUX. Clonal composition was determined by karyotyping, with fold expansion relative to day 35. **(I)** Clonal expansion of venetoclax-treated cultures subsequently treated with vehicle or RUX. Clonal composition was determined by karyotyping, with fold expansion relative to day 35.

Figure 1

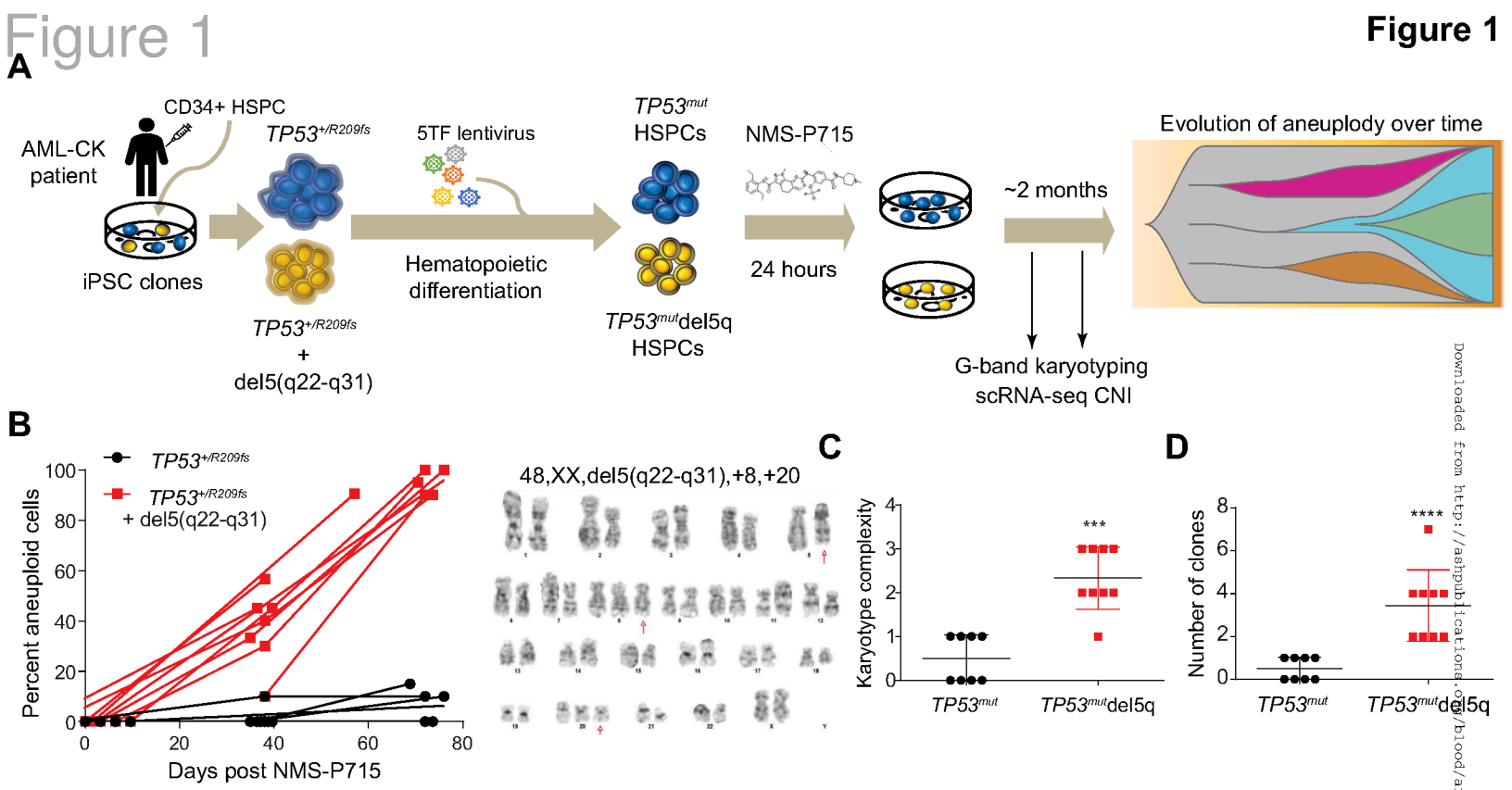

Figure 2

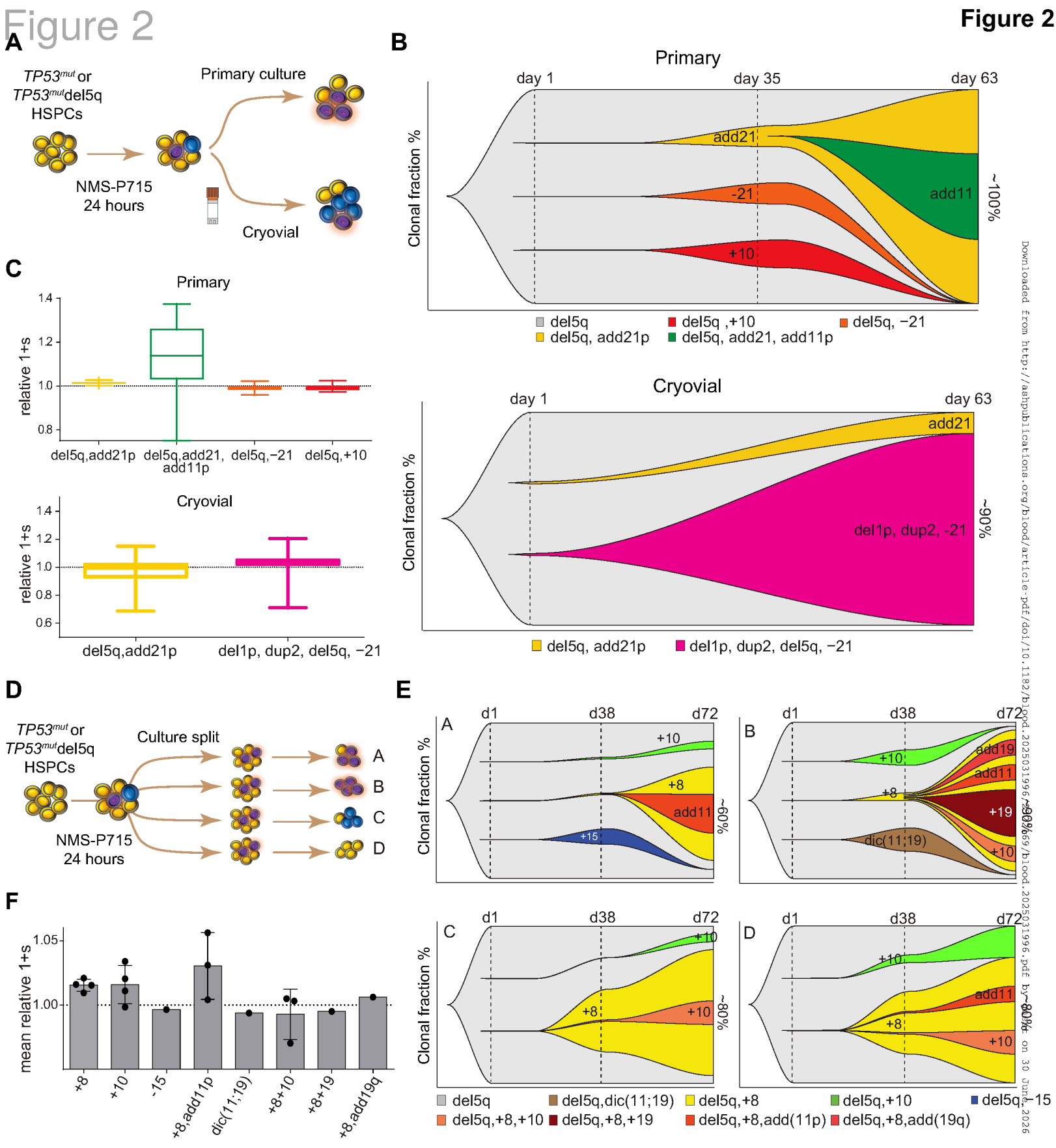

Figure 3

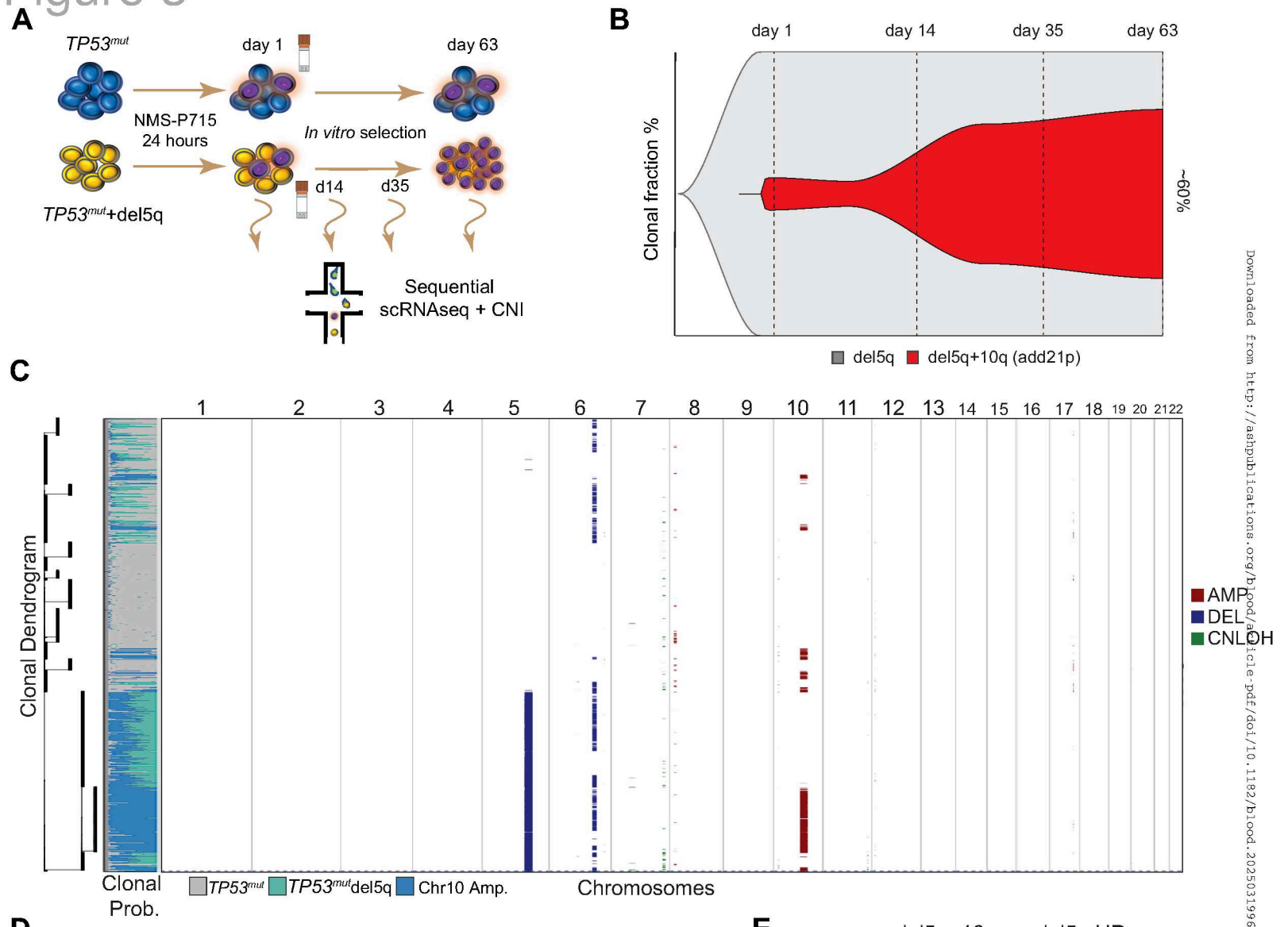

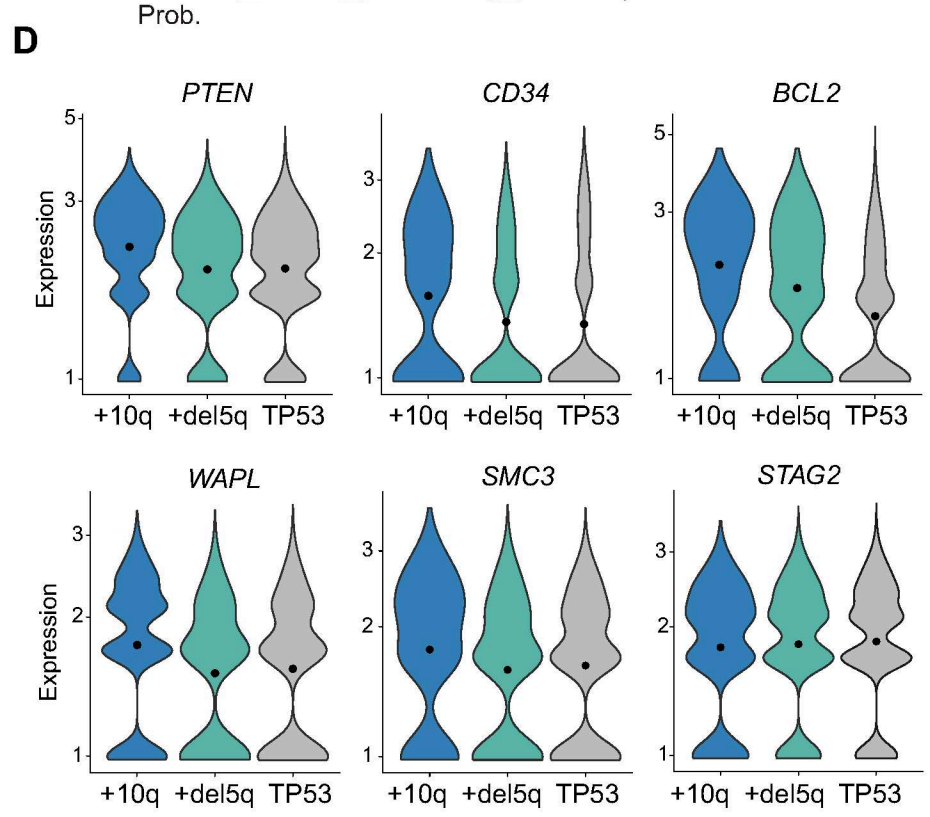

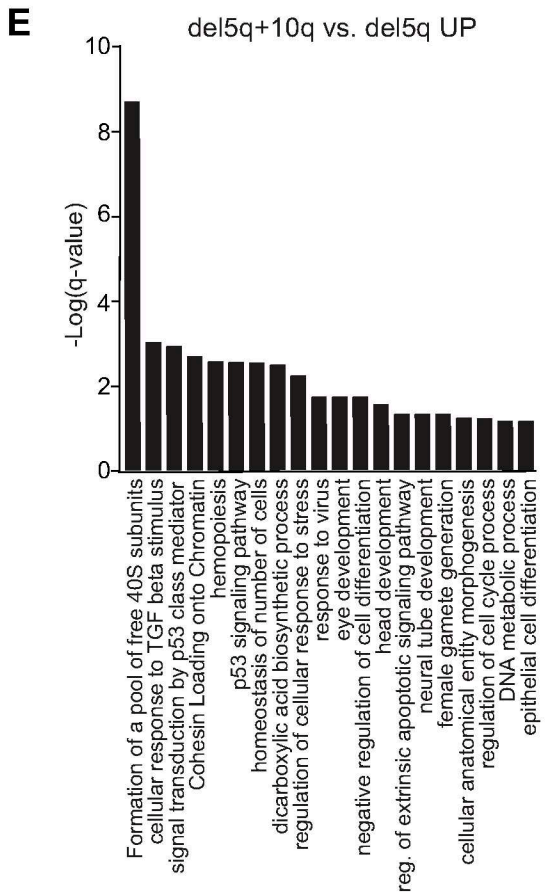

Figure 4

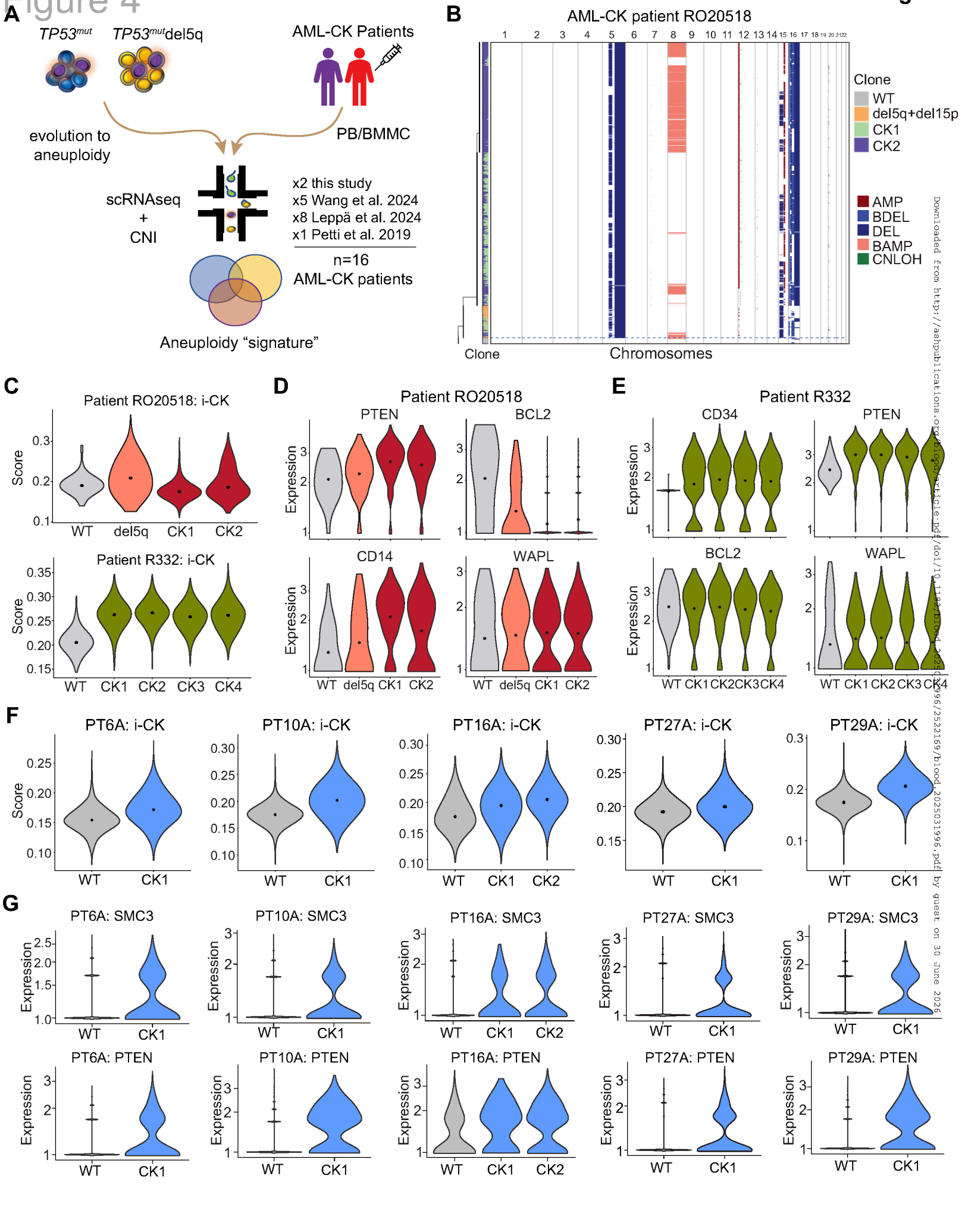

Figure 5

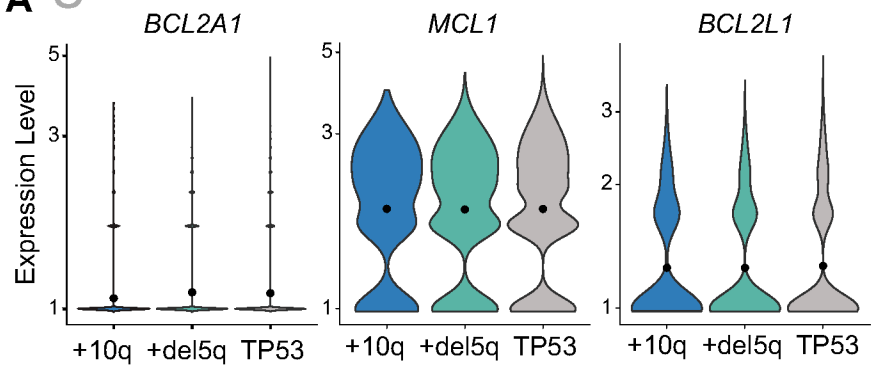

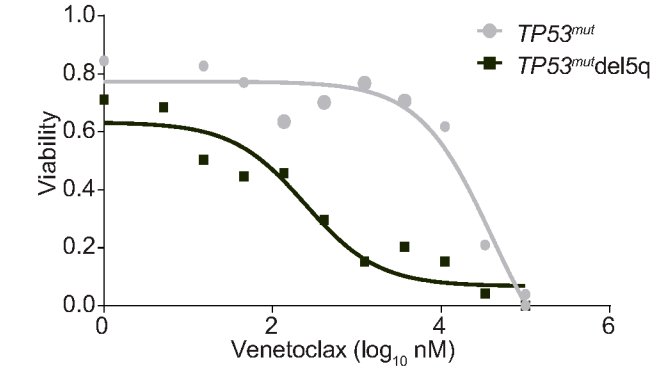

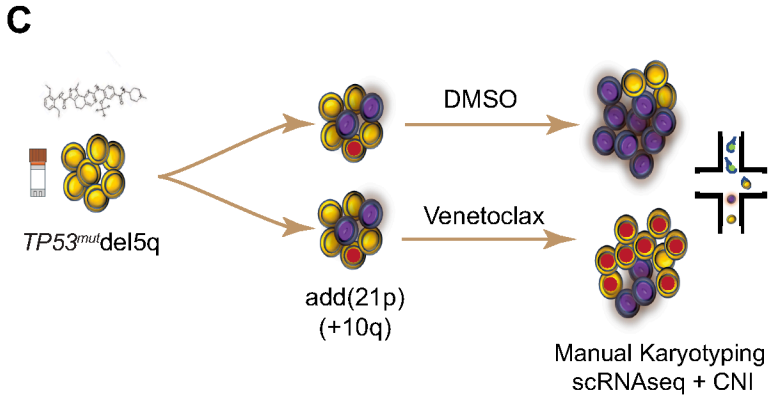

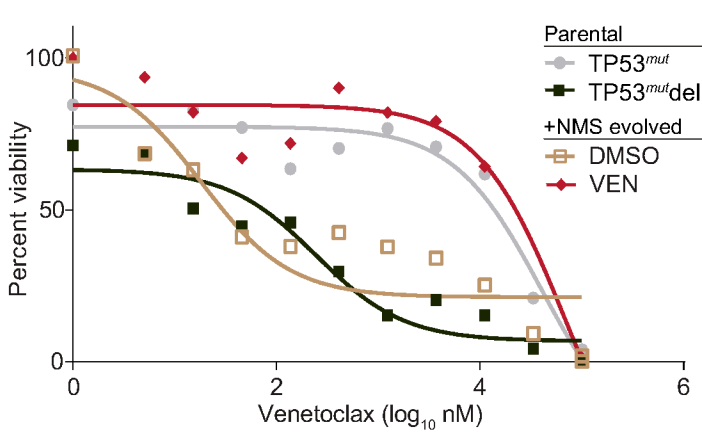

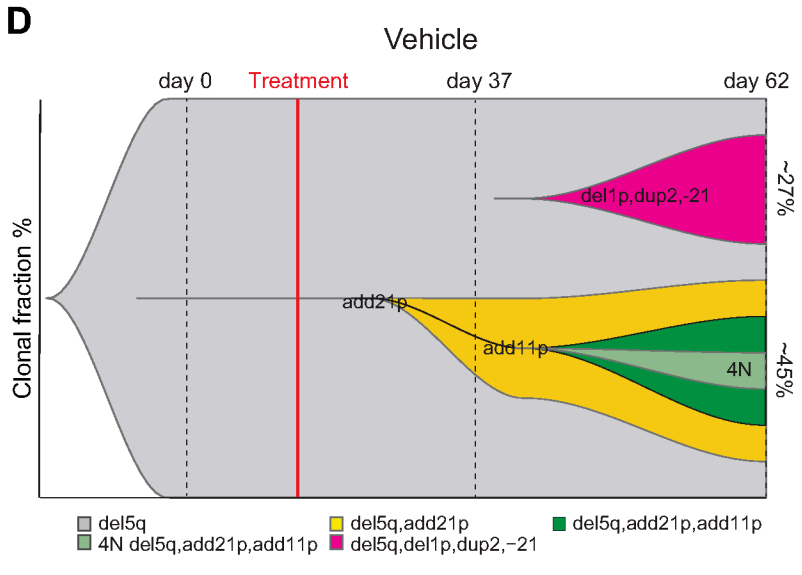

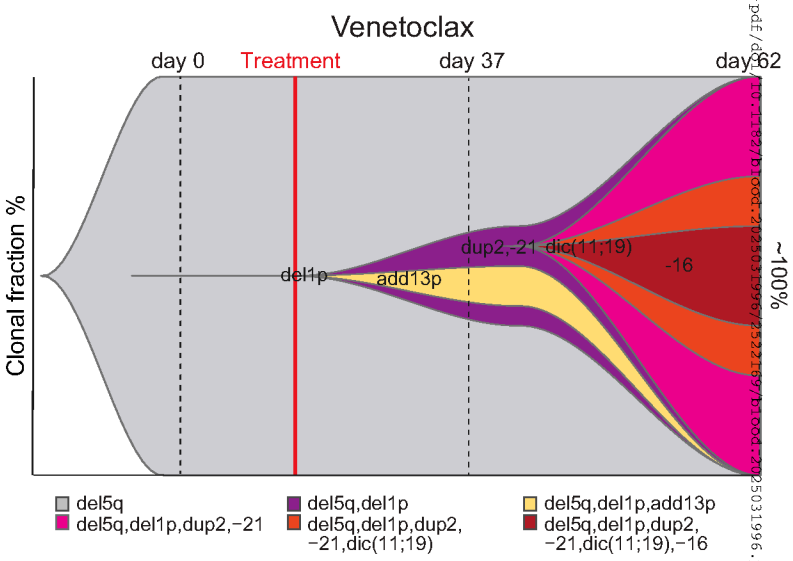

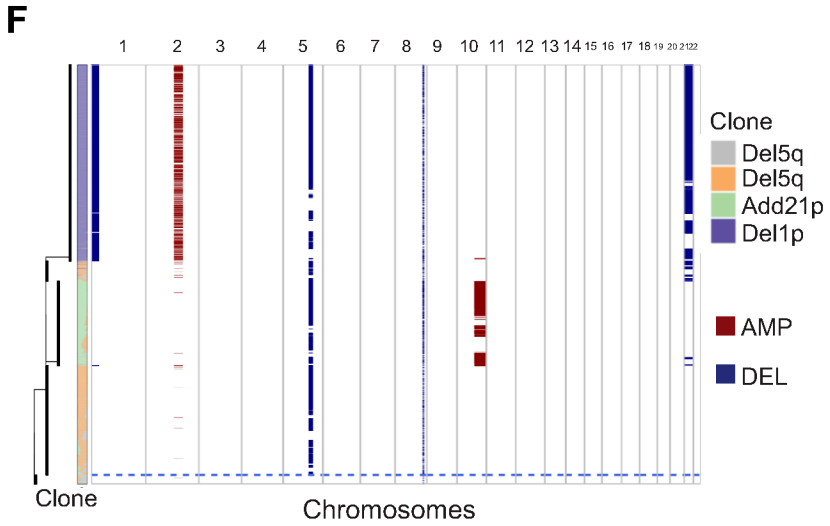

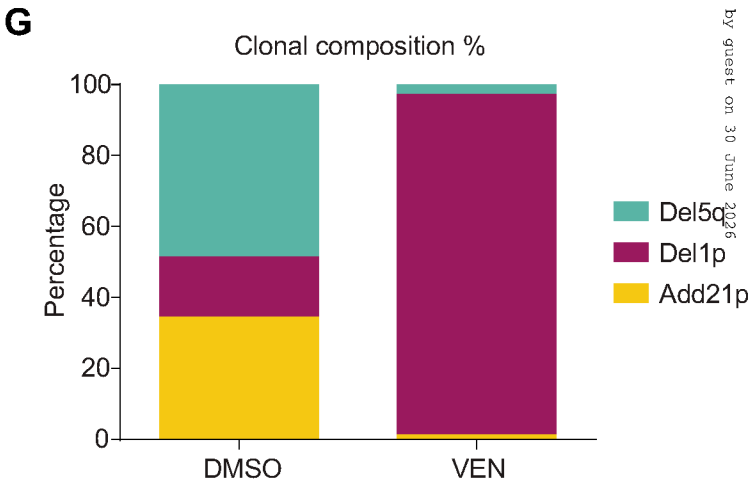

Figure 6